Heat flow in the Vøring Basin, Mid-Norwegian Shelf

Ulrich Ritter[1], Gary W. Zielinski[2], Hermann M. Weiss[1], Robyn L. B. Zielinski[2] and Joar Sættem[1, 3]

[1]*SINTEF Petroleum Research, NO-7465 Trondheim, Norway (e-mail: ulrich.ritter@iku.sintef.no)*
[2]*Omegalink International Ltd, 2382 Route 118, Dorchester, NH 03266, USA*
[3]*Present address: Miljø- og ubyggingsetaten, Sauherad kommune, NO-3812 Akkerhaugen, Norway*

ABSTRACT: *In situ* temperature and heat flow were determined in 1994 at 159 sites, grouped into 66 clusters between latitude 65° N and 67°30' N at water depths from 669 m to 1464 m. The mean of all cluster heat-flow measurements conducted in this survey was 58.5 mW m^{-2}, with a standard error of ± 4.40 mW m^{-2}. The mean heat flow from IKU well data for the Trøndelag Platform is 56.2 ± 6.65 mW m^{-2}. Shorter wavelength heat-flow variations appear to be controlled structurally and can be explained by sedimentation and thermal refraction effects. High heat flow associated with faulted structural highs such as the Nyk High and Vema Dome–Rym Fault Zone may also result from hydrothermal convection. Relatively isolated high (106.6 mW m^{-2}) heat flow observed at 846 m water depth may be an artefact of bottom water disturbances; however, virtually identical deep-water heat-flow anomalies, believed to be of hydrothermal origin, also exist. While heat-flow measurements made at water depths less than 1000 m should be regarded with caution, there is presently no justification for eliminating those exhibiting linear heat flow with depth. Submarine avalanches seem unimportant in the survey area. Neither crustal thinning, underplating nor sill intrusion, within the last 50 Ma, would have a measurable effect on present-day heat flow. The net effect of crustal thinning may be a reduction of the crustal heat generation potential, depending on the degree of thinning of the upper crust, since the accumulating sediments cannot compensate fully for the lost heat generation from a crystalline basement.

KEYWORDS: *heat-flow measurements, Vøring Basin, Norwegian shelf, thermal history*

INTRODUCTION

The Vøring Basin is a major deep-water frontier exploration area, which has been a focus of exploration during the last few years. Because of very long distances to well calibration data, and because the structural evolution of this area differs considerably from that of the better-explored Haltenbanken and North Sea, the temperature–depth relationships in the Vøring Basin have been uncertain. Previous heat-flow data from the area include gravity spear data reported by Haenel (1974), Langseth & Zielinski (1974), Zielinski (1977, 1979), Sundvor *et al.* (1989), and a single heat-flow value reported from ODP hole 644 (Eldholm *et al.* 1987, p. 650). Most of these have been discussed more recently by Vogt & Sundvor (1996) and Sundvor *et al.* (2000). Eighteen new heat-flow values derived from DST temperatures from deep wells of the Trøndelag Platform have been included in the discussion of areal heat flow.

Ever since Tissot & Espitalié (1975) first drew attention to the relation between heat flow and petroleum generation, research concentrated on the relationship between heat flow, hydrocarbon generation and migration (e.g. Zielinski & Bruchhausen 1983) and ever more refined kinetic models (e.g. Schenk *et al.* 1997) that link petroleum generation with temperature. Since then, research has resulted in several unique marine heat-flow datasets from global continental margins, funded by consortia of multinational exploration companies. The new data presented here are believed to be the first of such sets to be released for publication.

Sub-surface temperature is one essential parameter in modelling petroleum generation from source rocks, and can be inferred from measured surface heat flow. Heat flow tends to vary on both a small and a large scale. Most local exogenic processes are likely to extend only to shallow depth and, thus, do not affect source-rock maturation. Mantle-derived and refractive causes, in contrast, may last the life time of a basin. Fluid convection may enhance refraction effects but may be active for shorter time periods. The purpose of this paper is, therefore, to present the new heat-flow data, to discuss them in their regional context, to demonstrate which processes may influence their variability and, thus, to provide guidelines for explorationists on how to use heat-flow data.

TECTONIC HISTORY

The Vøring Basin area has been subjected to several tectonic episodes since the Caledonian orogeny in Ordovician–Silurian times (Brekke *et al.* 1999). After early crustal extension between the Carboniferous and Mid Jurassic, further extension occurred from Late Jurassic to Early Cretaceous with its axis in the

eastern part of the basin. In the Late Cretaceous a third phase of rifting occurred, leading to a break-up of the Norwegian–Greenland Sea around Paleocene/Eocene time. During the Tertiary the area developed as a volcanic, rifted margin with high sediment influx. Stuevold *et al.* (1992) observed several uplift events that helped strongly to shape the sedimentation pattern of the Vøring area. A Cretaceous–Paleocene uplift was associated with the formation of the volcanic margin. The Fennoscandian epeirogenic uplift probably took place from late Oligocene to the Pliocene and was followed by glacial rebound during the Holocene.

The Vøring Plateau marginal high is an integrated part of the North Atlantic Volcanic Province. In contrast to the central part near the Iceland hotspot, the volcanism at the Vøring Plateau was only transient and lasted about 3 Ma (Eldholm *et al.* 1989). The upper volcanic series has been dated to 54.5 Ma. It is composed of transitional mid-oceanic tholeiitic basalts, interbedded with thin volcaniclastic sediments. The lower series has been dated to 57.8 Ma and consists of dacitic flows, dykes and interbedded sediments (Eldholm *et al.* 1989). Skogseid *et al.* (1992) regard the Vøring area as a typical example of a 'volcanic continental margin', which is characterized by anomalous crustal thickness generated by magmatic underplating during a short, but intense period of rifting. They point out that the northeast Atlantic mantle plume affected a lithosphere that was already under extension. Hence, it did not start the rifting but led to increased generation of magmatic melt due to pressure reduction. Pedersen & Skogseid (1989) could show that only a minor temperature anomaly is required at the base of the lithosphere to explain the volume of basaltic magma and the amount of initial uplift observed at the Vøring Volcanic Margin. Present-day crustal profiles of the Vøring Basin show very strong attenuation of the isovelocity contours between 5 km s^{-1} and 6.5 km s^{-1} (e.g. Skogseid *et al.* 1992), while the contours between 6.5 km s^{-1} and 8 km s^{-1} appear to be less attenuated. This would suggest that the upper crystalline crust has undergone much stronger thinning than the lower crust. Van Schaack *et al.* (1998) discussed the lower crust of the Vøring area in terms of underplating, interpreting all P-wave velocities between 7.1 km s^{-1} and 7.5 km s^{-1} as igneous bodies consistent with magmatic underplating.

HEAT-FLOW MEASUREMENTS

During the 1994 IKU Vøring heat flow survey *in situ* temperatures and heat flow were determined at 159 sites, grouped into 66 'clusters'. Sediment cores were obtained from 56 sites, and 600 individual thermal conductivity measurements on these sediments were carried out aboard ship. The nomenclature used for the heat-flow measurement and cluster locations are given in Figures 1 and 2a, respectively.

The heat-flow data collection included shipboard thermal conductivity measurements via the needle probe method (Von Herzen & Maxwell 1959), performed on gravity corer samples. Thermal gradient measurements were obtained by four outrigger-mounted thermistor probes attached to 3.5 m and 4 m long gravity spears. Temperatures were recorded *in situ* by digital thermograds and read out onto computer between measurement intervals. Data from the thermograds were used to establish equilibrium temperature at each of the four depth points. The vertical flux of heat through the sea-floor sediments was obtained by combining the site thermal conductivity value (K) with the thermal gradient value (dT/dZ) for the corresponding depth interval, in scalar form:

$$HF = K\frac{dT}{dZ} \tag{1}$$

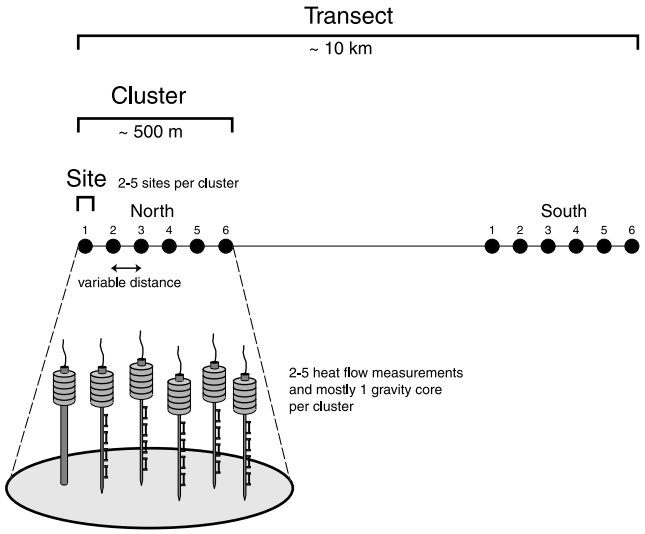

Fig. 1. Sampling pattern and nomenclature used in this study.

Thermal conductivity measurements were performed on equilibrated sealed sections of jacketed cores with the needle probe orientated perpendicular to the axis of the core. A site/cluster thermal conductivity was obtained from the harmonic means of values for multiple depths in each core and then corrected for *in situ* temperature and pressure (Ratcliffe 1960). Heat flow was then computed using the same value of thermal conductivity for each site within a cluster.

RESULTS

A summary of the results of the 1994 Vøring heat-flow project is given in Table 1. Additional heat-flow values from deep wells of the Mid-Norwegian Shelf, determined using drill stem test (DST) temperatures and an IKU-internal thermal conductivity database, are given in Table 2. Figure 2a shows the main structural features, water depth, IKU cluster locations and the site numbers of Sundvor *et al.* (1989) and Figure 2b shows the average heat-flow values for these clusters and sites. Table 1 also gives the uncertainty of the heat-flow determinations on the 1σ level. Assuming that temperature gradient and thermal conductivity vary independently, cluster heat flow (HF_c) is:

$$HF_c = (K_c \pm \sigma K_c)(GR_c \pm \sigma GR_c) \tag{2}$$

and

$$\sigma HF_c = GR_c \sigma K_c + \sigma GR_c K_c \tag{3}$$

where σHF is the heat-flow uncertainty within the cluster at the 1σ level; K_c is average cluster thermal conductivity, σK_c is the standard deviation of the conductivity measurements obtained in the cluster (about 12 to 15 measurements); GR_c is the average cluster temperature gradient and σGR_c is the standard deviation of all temperature gradients taken at the cluster.

Heat-flow uncertainties in Table 2 have been estimated from DST temperatures and an assigned variability of thermal conductivity (usually one standard deviation) from the internal database of the units overlying the DST measurement. The Jurassic (Table 2), for example, has relatively variable lithology and, hence, conductivity also varies strongly. Parts of the Tertiary and the Upper Cretaceous consist of monotonous shale and sandy shale, and the uncertainty of conductivity is, therefore, small. Weighted means of conductivity and its variability were then used to calculate heat flow and its uncertainty. Temperature uncertainties are assumed to be negligible since most of the temperatures are taken from DSTs.

Among the Table 1 data, the highest gradient uncertainty (σGRc) was found for cluster 26 N which consists of five individual thermograd measurements. If a single very low gradient value (21.4 mK m^{-1}) is omitted, the gradient uncertainty for the remaining sites drops to 1.29 mW m^{-1} for a mean gradient of 68.00 mK m^{-1}. This results in a well-determined cluster heat flow of 88.5 mW m^{-2}. Very low thermal gradients and heat flow, as observed at the single 26 N site, are known to occur within zones of high heat flow (e.g. Von Herzen & Uyeda 1963; Lee & Uyeda 1965; Zielinski *et al.* 1990); hence, the high uncertainty for 26 N and the other clusters of sites in Table 1 can be interpreted generally as the variability of the respective gradient, thermal conductivity and heat flow at that location. High variability in thermal conductivity (σKc) can be interpreted as indicating a high local vertical variability of lithology, possibly relating to changes in depositional environment, or a random high number of needle-probe measurements performed in zones of vertical lithological transition. In any case, the variability in thermal conductivity is small compared with that for gradient and heat flow, and the effect of averaging performed on the individual thermal conductivity measurements serves to lessen any effect on the heat-flow results.

Heat flow, temperature gradient and thermal conductivity are all skewed towards higher values (Fig. 3). Omitting heat flow from clusters less than 1000 m deep lowers the modal heat-flow value by about 5 mW m^{-2} (Figs. 3a, b). A weak skewness of the thermal gradient distribution (Fig. 3c) is a necessary consequence of the strongly skewed thermal conductivities (Fig. 3d). Skewness toward high values of heat flow (Fig. 3) is a ubiquitous feature of the global heat-flow database (Lee & Uyeda 1965).

The shallow probe heat-flow measurements are listed in Table 1. Heat-flow values from deep wells are listed in Table 2. Notably absent in the deep well data are the higher (>70 mW m^{-2}) values present in the shallow probe data. In other respects, however, the two datasets are in remarkable agreement, even without eliminating the high uncertainty clusters from the shallow probe data. This observation can only increase confidence in the data results.

The heat-flow anomaly extending from the Någrind Syncline to the Vøring Marginal High (Fig. 2b) consists mainly of heat-flow values from Sundvor *et al.* (1989). In the northwest the latter appear to be around 10 mW m^{-2} higher than IKU measurements in the vicinity (6S, 6 N). More towards the southeast, the IKU and Sundvor *et al.* (1989) data tend to show better agreement. Eldholm *et al.* (1987) quoted a heat flow of 61 mW m^{-2} for ODP site 644, which is in good agreement with the regional average from this study for the shallow probe data (Table 1).

In summary, the general pattern of heat flow is broadly in line with the general structural grain. It is interrupted by small patches of particularly high heat flow, which in some cases appear to be orientated perpendicular to the general strike.

FACTORS THAT MAY INFLUENCE HEAT FLOW

The main exogenic factors that may influence heat-flow variation in this area may result from Plio-Pleistocene sedimentation rate, bottom water temperature variations, and sea bottom disturbances, such as large-scale submarine slides, which are known to have occurred in the area (e.g. Bugge *et al.* 1987). The main endogenic factors may result from variation of crustal heat generation, sediment–basement thermal conductivity contrasts, large-scale water convection, residual heat from intrusion of magmatic rocks, magmatic underplating and rifting. Attempts are made in the following to estimate the impact of each of these mechanisms as a guideline for interpreting the heat-flow pattern of the Vøring area.

Exogenic causes of heat flow variation

Sedimentation rate. Rapid sedimentation may lead to a lower geothermal gradient (Von Herzen & Uyeda 1963). The effects of rapid sedimentation have been tested using a vertical 1D heat conduction model (software BasinMod™) for possible Quaternary subsidence histories and average thermal properties. In the example in Figure 4a the thermal gradient (about 55°C km^{-1}) will be reduced by about 24°C km^{-1} if an accumulation rate of 2500 m Ma^{-1} is maintained for some time and the accumulation rate is infinitely low. Even rather short interruptions of sediment accumulation will lead to a rapidly rising gradient (Fig. 4b).

In the area investigated, Plio-/Pleistocene sediment thickness varies between 50 m and 1800 m. If all these sediments accumulated during the last 1 Ma, the thermal gradient would be lowered to a maximum of about 70% of the steady-state value, and about 90% of the steady-state value if the sediments accumulated since 2.6 Ma, as dated at ODP site 644 (Eldholm *et al.* 1989). Any periods of non-deposition would reduce this difference further (Fig. 4b). Judging from Figure 5, Plio-/Pleistocene sedimentation should be strongest around km 200, while the most recent Quaternary sediments are thickest further to the east at the Træna Basin. The lowest heat flow encountered in this area is in well 6607/5-1 at 43 mW m^{-2}, where the Plio/Pleistocene thickness is around 1000 m (Fig. 5, 210 km). Here, from Figure 4, suppression of heat flow from late sedimentation should be around 20%. This would correspond to a background heat flow of 55 mW m^{-2}, which is in agreement withVon Herzen & Uyeda (1963, fig. 9). Hence, this mechanism appears fully capable of accounting for any low heat flow observed in these data, except for the single very low value of 28 mW m^{-2} at 26 N, discussed earlier.

Bottom water. Water temperature along the Norwegian Shelf tends to experience short-term (monthly, annually), as well as long-term (decades), changes (e.g. Gammelsrød & Holm 1984; Gammelsrød *et al.* 1992). Variability is largest at water depths less than 900 m; whereas, at a depth of more than 1000 m, long-term variation of water temperature seems to be extremely small (Gammelsrød *et al.* 1992). Measurements at 66° N/2° E (Gammelsrød & Holm 1984) suggest decreasing temperatures from about 1970 to 1980 (Fig. 6a). Figure 6c shows schematically the transitional gradient resulting from cooling of the sediment surface.

The transient effects of water temperature variation down to a depth of a few metres were modelled using these data. The results for different water depths and probe penetration are given in Figures 6b and d. The vertical axes show the resulting deviations from the measured gradients for penetration depths of 0 m, 3.5 m, 30 m and 70 m. Figure 6d is computed using the whole water temperature history up to 1994 and is, thus, representative of that year's IKU measurements. Figure 6b is based on the history up to 1985 and is, thus, representative of the Sundvor *et al.* (1989) data. Both figures show that there is no significant thermal disturbance from bottom water variation at more than 1000 m and for penetration depths greater than about 5 m.

The effects seen in Figures 6b and d are out of phase since the 1994 IKU data were obtained at a time of cooling of bottom waters (Fig. 6a), whereas the Sundvor *et al.* (1989) data were obtained during a time of bottom water warming. For the IKU survey, Figure 6c predicts a mean increase in gradient of

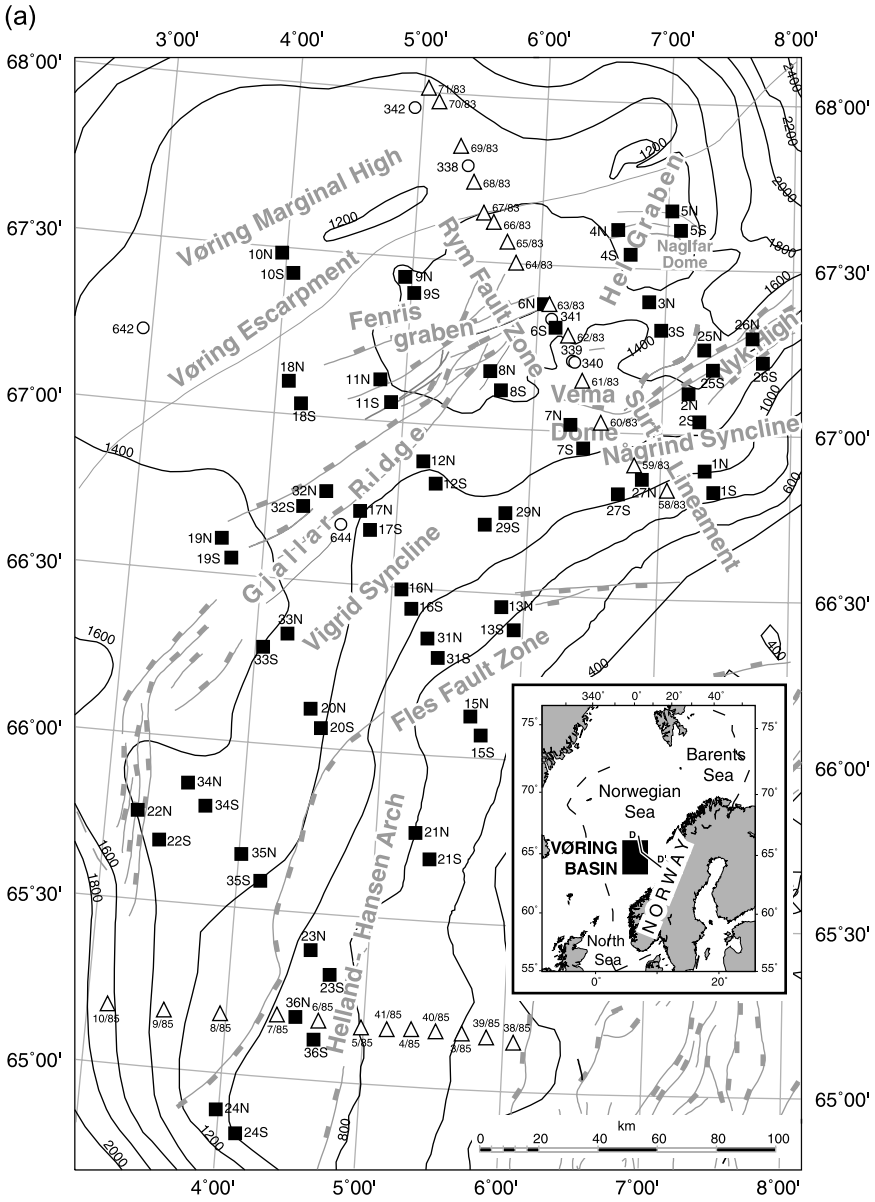

Fig. 2. (**a**) Main structural features, water depth (in m) and shallow heat-flow sites. Solid squares, IKU sampling clusters with cluster ID; open triangles, Sundvor *et al.* (1989) sites; open circles, ODP drill sites. Inset: location of the area investigated. D–D' is the profile in Figure 5.

about 70 mK m^{-1} in the 0–3.5 m sediment interval at 600 m water depth. This is equivalent to about a 70 mW m^{-2} increase in heat flow. The shallowest heat-flow measurements from the study (Table 1) are in waters not much deeper than 600 m. The implication for the data is that heat-flow values in excess of 100 mW m^{-2} at water depths less than 1000 m may be indicative of bottom water disturbance. At the same time, one should realize that such anomalies also occur at deep-water sites (e.g. Sundvor *et al.* 1989, figs 2a, b) where they are unlikely to be caused by bottom water disturbances (Vogt & Sundvor, 1996; Sundvor *et al.* 2000).

However, in this study, only one isolated cluster heat-flow value in excess of 100 mW m^{-2} (106.6 mW m^{-2}) at a water depth of 846 m (13 N, Table 1) was observed, which is based on two gradient measurements. Furthermore, the mean heat flow for the 11 clusters at water depths less than 1000 m, excluding 13 N, is 61.7 mW m^{-2}. This value is not significantly greater than that for the entire Table 1 dataset (58.5 mW m^{-2}) or the 61 mW m^{-2} value obtained at ODP site 644 (Eldholm *et al.* 1989). Hence, it is unlikely that the data at shallow depths from this study are affected by anywhere near the magnitude predicted by modelling the Gammelsrød & Holm (1984) hydrographic data. It is possible, however, that the 2.5 times higher standard deviation (11.2) for the 11 shallow heat-flow values in Table 1 may be indicative of bottom water disturbance, and some degree of caution may be warranted.

Submarine slides. Large-scale submarine slides were reported from the Norwegian Shelf (Storegga slides) by Bugge (1983) and Bugge *et al.* (1987). The Storegga slides occurred about 25 000 and 7000 years ago, either removing or depositing sediments of several tens of metres thickness. They are likely to have resulted in a disturbance of the temperature gradient near the surface of the sediments, which, by today, may not yet have dissipated fully. The effect of a sudden deposition of a sedimentary layer on surface heat flow has been modelled by Von Herzen & Uyeda (1963). For thicknesses of 10 m to 100 m the thermal disturbance was found to be significant for 10^2 to 10^4 years. Heat-flow measurements performed at the sediment surface in such an area should, therefore, be viewed with caution. Only minor submarine slides appear to affect the area of investigation (T. Bugge, pers. comm. 1998). Clusters 25 N and 34 may have been affected by slide activity but show no obvious signs of heat flow disturbance (Fig. 2b).

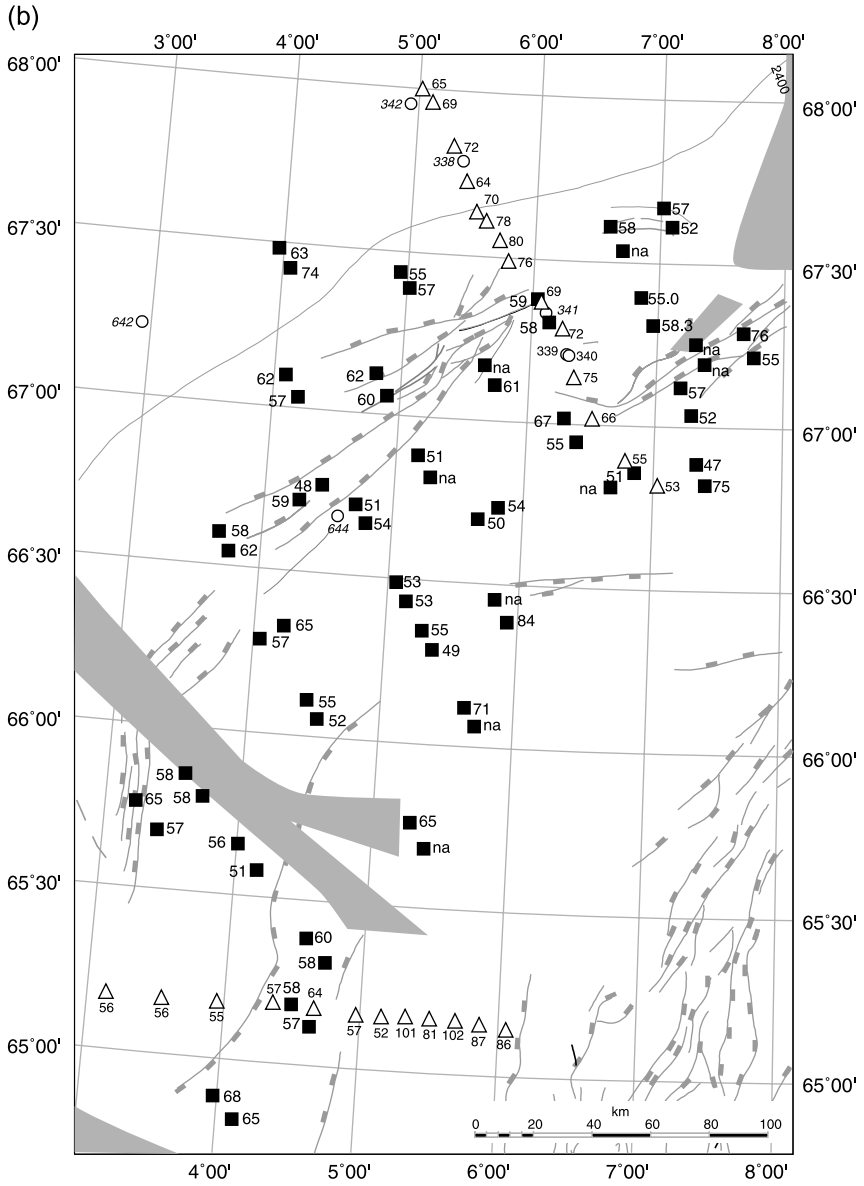

Fig. 2. (**b**) Average heat flow (in mW m^{-2}) for each cluster. For structure names and cluster IDs see (a). Areas of possible submarine slides are shaded. na, clusters with insufficient data to compute a parameter.

Endogenic causes of heat flow variation

Heat generation. The steady-state heat flow observed at the Earth's surface is derived from the mantle as well as from the radiogenic heat production of crystalline basement and the sediments. The contributions to steady-state surface heat flow from mantle, crust and sediments have been evaluated using a vertical heat generation profile that sums the respective contributions to surface heat flow:

$$HF_s = HF_m + HF_{cc} + HF_{ss} \quad (4)$$

where HF_s is the surface heat flow, HF_m is the mantle heat flow, in all scenarios set to 25 mW m^{-2}. HF_{cc} is heat generation from the crystalline basement, HF_{ss} is the heat generation from the sedimentary cover:

$$HF_{ss} = \sum_0^z A_s dz \quad (5)$$

where A_s is sedimentary heat generation derived from API logs after Buntebarth (1980) and individually assigned to rock types or lithological units. The distribution of heat generation within the crystalline crust is calculated in some cases using

$$A(z) = A_0 e^{-z/D} \quad (6)$$

and

$$z = \frac{C_u}{\beta} + C_l \quad (7)$$

where z is depth below top of basement, C_u is thickness of upper crust (20 km), β is crustal thinning factor (McKenzie 1978); D=10 km, slope parameter (Lachenbruch & Sass 1977, equation (22)); A_0 is the heat generation at top of basement, and C_l is thickness of the lower crust (10 km), a constant.

Integrating $A(z)$, heat flow contributed from the crystalline basement becomes

$$HF_{cc} = A_0 D(1 - De^{-z/D}) \quad (8)$$

The mantle heat flow and the slope factor D have been chosen to be in close agreement with the heat generation versus heat flow plotted for the Precambrian of southern Norway (Heier & Grønlie 1977), assuming a similar basement

Table 1. *IKU heat flow data collected in 1994*

CL	WD (m)	GR_c (mK m^{-1})	σGR_c (mK m^{-1})	K_c (W m^{-1} K^{-1})	σK_c (W m^{-1} K^{-1})	HF_c (mW m^{-2})	σHF_c (mW m^{-2})	Remarks
01 N	993	48.10	na	0.99	0.02	47.4	na	
01S	853	61.00	3.25	1.23	0.01	74.8	4.38	
02 N	1344	56.75	1.48	1.00	0.02	56.5	2.74	K_c from 02S
02S	1238	51.90	3.54	1.00	0.02	51.7	4.67	
03 N	1421	52.55	5.02	1.04	0.03	54.8	6.94	
03S	1419	55.85	1.77	1.04	0.03	58.3	3.65	K_c from 03 N
04 N	1289	62.40	1.66	0.93	0.02	58.2	2.89	
04S	1302	58.67	2.05	*0.93*	*0.02*	*54.6*	*3.17*	K_c from 04 N
05 N	1271	55.60	11.27	1.02	0.02	56.5	12.46	
05S	1304	55.50	2.60	0.93	na	51.7	na	
06 N	1451	61.00	2.55	0.96	0.02	58.5	4.12	
06S	1424	62.80	na	0.93	0.01	58.2	na	
07 N	1227	69.20	na	0.96	0.02	66.6	na	
07S	1202	53.90	6.08	1.01	0.02	54.5	7.28	
08 N	1408	55.35	1.77	*0.99*	*0.02*	*54.8*	*2.63*	K_c from 08S
08S	1388	61.25	2.19	0.99	0.02	60.8	3.14	
09 N	1372	57.15	2.19	0.96	0.02	54.6	3.29	
09S	1395	59.70	7.21	0.96	0.02	57.0	8.14	K_c from 09 N
10 N	1206	62.50	2.55	1.00	0.01	62.6	3.44	K_c from 10S
10S	1200	73.80	na	1.00	0.01	73.9	na	
11 N	1361	65.80	0.00	0.95	0.01	62.4	0.93	
11S	1360	62.25	2.19	0.96	0.01	59.5	2.91	
12 N	1206	53.80	3.25	0.95	0.01	50.9	3.85	
12S	1161	53.10	0.71	*0.95*	*0.01*	*50.4*	*1.43*	K_c from 12 N
13 N	846	96.90	na	*1.10*	*0.03*	*106.6*	na	K_c from 13S
13S	741	76.70	na	1.10	0.03	84.1	na	
15 N	669	76.00	na	0.93	0.01	70.9	na	
15S	660	nl	na	0.95	0.05	na	na	gradient non-linear (nl)
16 N	1071	58.65	2.19	0.91	0.01	53.2	2.48	
16S	1027	59.45	1.77	0.88	0.01	52.6	2.00	
17 N	1194	54.04	3.05	0.94	0.02	50.7	4.21	
17S	1156	56.78	4.01	0.95	0.01	53.7	4.53	
18 N	1374	65.20	0.28	0.95	0.03	62.1	2.28	
18S	1359	63.65	4.74	0.90	0.01	57.3	5.00	
19 N	1430	63.30	0.00	0.92	0.01	58.0	0.77	
19S	1440	63.25	1.48	0.99	0.01	62.4	2.23	
20 N	1229	57.40	6.08	0.96	0.01	54.9	6.59	
20S	1182	54.35	2.47	0.95	0.03	51.6	3.86	
21 N	762	68.60	18.38	0.95	0.02	65.4	19.18	
21S	704	nl	na	1.12	0.06	na	na	gradient non-linear (nl)
22 N	1389	64.55	6.15	1.01	0.02	65.0	7.30	
22S	1355	59.95	1.77	0.94	0.01	56.5	2.05	
23 N	928	66.30	na	0.90	na	59.8	na	
23S	844	61.70	na	0.94	na	58.1	na	
24 N	1098	88.20	0.57	0.77	na	68.3	na	
24S	1011	81.40	3.25	0.80	na	65.2	na	
25 N	1530	55.65	3.61	*1.10*	na	*61.2*	na	K_c from 2 N, 3S, 26 N, 26S
25S	1424	54.35	2.47	*1.10*	na	*59,8*	na	K_c from 2 N, 3S, 26 N, 26S
26 N	1460	58.68	20.87	1.30	0.25	76.4	na	see text for discussion
26S	1203	51.76	2.71	1.05	0.03	54.5	4.21	
27 N	1043	54.60	1.41	0.93	0.01	50.9	1.86	
27S	1019	na	na	na	na	na	na	
29 N	1024	55.30	2.55	0.98	0.01	54.0	2.84	
29S	1103	52.60	na	0.95	0.02	50.0	na	
31 N	939	61.75	2.90	0.89	0.01	55.1	2.99	
31S	852	55.40	na	0.88	0.01	48.5	na	
32 N	1282	50.50	1.41	0.95	0.02	48.0	2.32	
32S	1299	58.85	3.18	1.01	0.02	59.3	4.56	
33 N	1359	63.75	2.90	1.01	0.02	64.5	4.29	
33S	1386	54.65	0.07	1.04	0.03	56.9	1.46	
34 N	1374	63.30	0.00	0.91	0.01	57.5	0.37	
34S	1352	61.70	0.71	0.94	0.02	57.9	1.71	
35 N	1242	59.70	8.63	0.94	0.02	56.3	9.25	
35S	1160	54.10	7.21	0.93	0.01	50.5	7.34	
36 N	945	67.90	na	0.85	na	57.8	na	
36S	904	64.80	na	0.87	na	56.6	na	
		61.0	*3.60*	*0.97*	*0.02*	*58.5*	*4.4*	*arithmetic mean of population*

CL, cluster; WD, water depth; GR_c, geothermal gradient, cluster average; σGR_c, standard deviation of cluster gradient; K_c, thermal conductivity, cluster average; σK_c, standard deviation of K; HF_c, heat flow, cluster average; σHF_c, heat-flow uncertainty in cluster, 1 sigma level. na, clusters with insufficient data to compute a parameter. Underlined values omitted from statistical treatment.

Table 2. *Heat-flow values estimated from deep wells*

Well	*HF* (mW m^{-2})	*HF* uncertainty (mW m^{-2})	Sample age	Depth below mean sea-level (m)
6201/11-1	60.3	3.7	U Triassic	2365
6407/2-3	58.5	3.7	U Jurassic	2194
6407/7-1S	58.5	3.6	Jurassic	2712
6407/7-2	60.3	3.7	U Jurassic	2477
6407/7-3	58.7	3.8	L M Jurassic	2575
6407/9-1	55.8	3.7	U Jurassic	1362
6407/9-4	50.9	3.3	U Jurassic	1389
6407/9-5	60.9	4.0	U Jurassic	1304
6506/12-5	51.9	3.1	Jurassic	3678
6506/12-6	50.0	2.7	U Jurassic	4307
6506/12-7	52.3	3.4	M U Jurassic	4344
6507/7-5	46.3	3.0	M Jurassic	2025
6507/7-6	50.4	3.9	L Jurassic	2012
6607/5-1	43.0	2.6	U Cretaceous	3425
6609/7-1	66.2	4.5	Permian	1671
6609/11-1	62.1	5.1	U Triassic	2805
6610/7-1	67.8	4.6	U Triassic	3040
6610/7-2	58.2	4.2	M Triassic	3058
Mean population	56.2	3.72		
Standard deviation	6.65			

HF is the heat flow calculated from the mean thermal conductivity and the measured DST temperature. 'Sample age' gives the stratigraphic unit where temperature has been measured, and 'Depth below sea-level' the respective sediment depth.

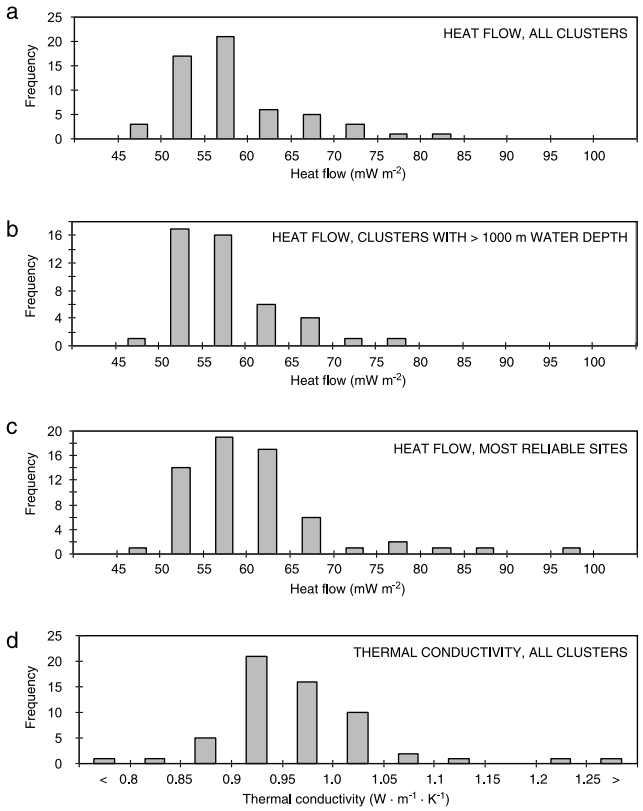

Fig. 3. Statistical overview of IKU Vøring heat flow data, based on data in Table 1. See text for further discussion.

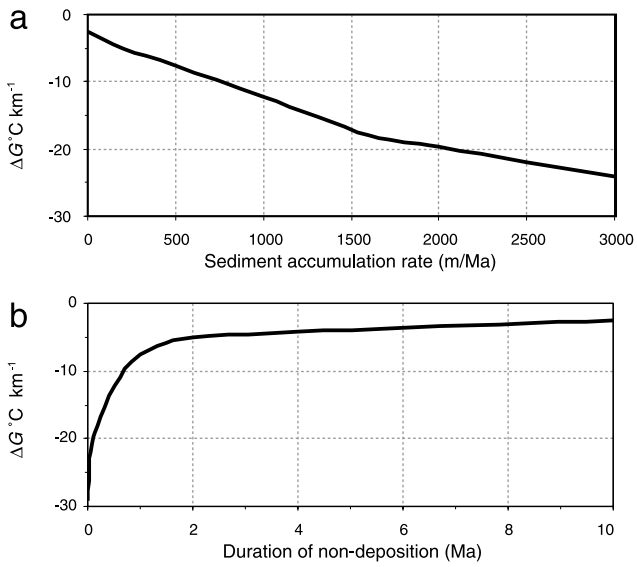

Fig. 4. Transient effects of Quaternary sediment accumulation and non-deposition on temperature gradient. Calculation using the transient heat-flow option in software BasinMod™ for an arbitrary background heat flow. ΔG is the deviation from the steady-state gradient (here *c.* 55 °C km^{-1}). All gradients are calculated for 200 m below sediment surface. (**a**) Effect of sediment accumulation rate; (**b**) effect of non-deposition, calculated using an accumulation rate of 3000 m Ma^{-1} prior to non-deposition. Immediately after deposition ΔG is about 25 °C km^{-1} and decays rapidly during the first 2 Ma of non-deposition when it reaches about 50 °C km^{-1}.

composition below the Palaeozoic rocks of Mid Norway. Crustal thinning factors were estimated using deep crustal seismic and gravity data.

The three different heat-flow scenarios shown in Figure 5 are based on different assumptions of heat generation within the crust. Scenario A was calibrated using a Helgeland Basin heat flow of 62 mW m^{-2} and further calibrated by setting crystalline basement heat generation A_0 to 3.65 μW m^{-3}, and β to 5.5 between km 140 and 320. Scenario B was calibrated using a Helgeland Basin heat flow of 61.4 mW m^{-2}. The heat generation of the upper crystalline basement was kept constant at 1.4 μW m^{-3}. The lower crystalline basement (>20 km) was assigned a constant heat generation of 0.1 μW m^{-3}; β was 5.5 between km 140 and 320. In Scenario C crystalline basement heat generation was derived using the V_P–heat generation relationship from Cermak *et al.* (1990) and seismic velocities for the area from Skogseid *et al.* (1992). The rationale for using different scenarios of heat generation is that with increasing

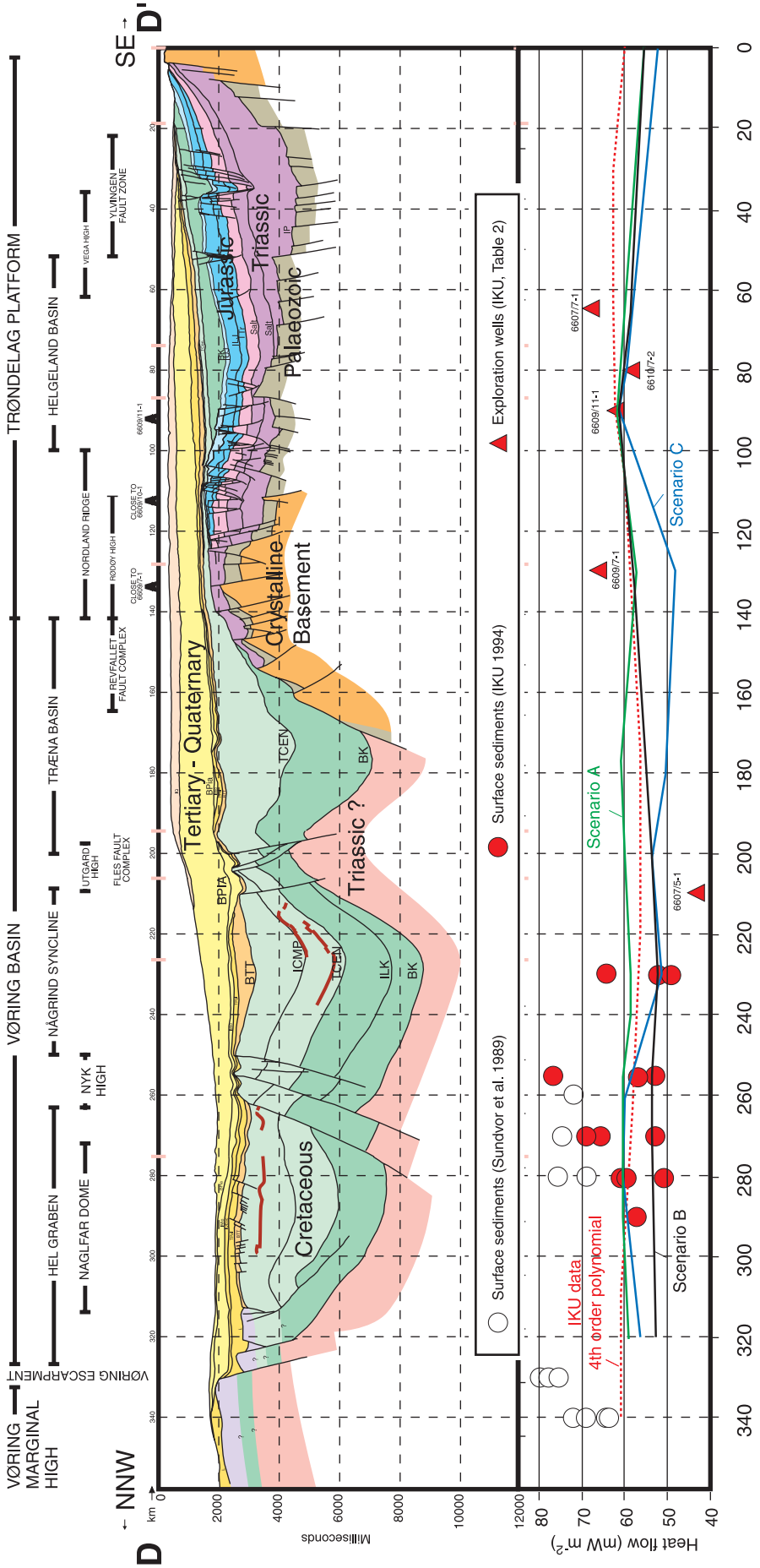

Fig. 5. Profile D–D′ from Blystad *et al.* (1995). Measured and estimated steady-state heat flow for three different scenarios (see text for further explanations). For location of the profile see the key map in Figure 2a.

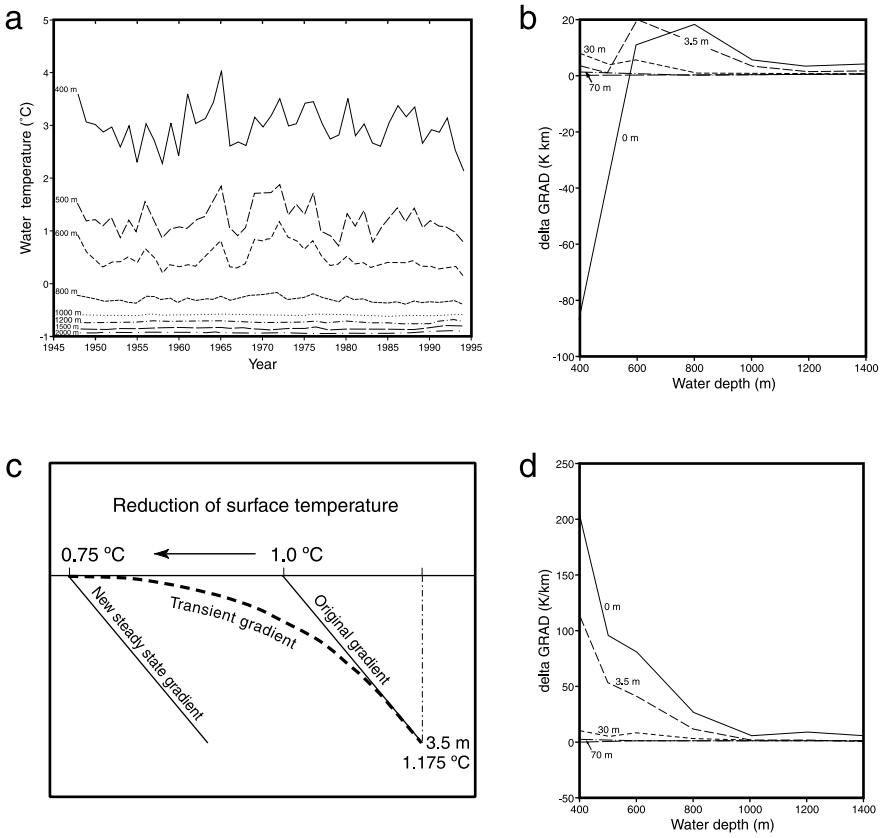

Fig. 6. Bottom water temperature histories and modelled deviations of sediment thermal gradient. (**a**) Water temperature histories 1945–1995, measured at various water depths at 66° N/2° E (Gammelsrød & Holm 1984; Gammelsrød *et al.* 1992). (**b**) Deviation of temperature gradient (delta GRAD) from steady state resulting from the water temperature histories in (a). Deviations are shown for different penetration depths. The diagram includes the history up to 1985 and is, thus, representative for the data of Sundvor *et al.* (1989). (**c**) Effects of near-surface gradients. A reduction of surface temperature increases the gradient. (**d**) As in (b). The diagram includes the entire history up to 1994 and is, thus, representative for the IKU measurements. A sediment thermal diffusivity of 2×10^{-3} cm^2 s^{-1}, a thermal conductivity of 1.0 W m^{-1} K^{-1} and a thermal gradient of 50 °C km^{-1} are assumed.

crustal depth, crystalline rocks tend to become more mafic, either gradually or step-wise, reducing the amount of radiogenic elements, particularly potassium. If the broad range of rock types present in the middle and lower crystalline crust are then inferred from seismic and gravity data, their contribution to surface heat flow can be estimated. The heat-flow values used for calibration are averages taken from the Mid-Norwegian mainland between 64° N and 66° N (Hurtig *et al.* 1992) or the Trøndelag Platform (Fig. 2b, Table 2) where conditions are likely to be in a steady state. If large-scale crustal water circulation occurs in these areas, the amounts of heat transported are probably small since the volumes of sediments and, thus, of expelled water, are also small.

Figure 5 combines cross-section D from Blystad *et al.* (1995) with measured and modelled heat flow at or near the section. The diagram shows IKU cluster averages, heat flow from deep wells (Table 2) and heat-flow values from Sundvor *et al.* (1989). A fourth-order polynomial was calculated from Table 1 data and crystalline basement heat-flow values from the Norwegian mainland (Hurtig *et al.* 1992), with heat flow set to 60 mW m^{-2} at km 0 and at km 340. In all scenarios the modelled steady-state heat flow decreases towards the deep parts of the basin. This is to be expected since the upper crystalline basement, the main heat-generating layer, is being thinned by a factor of 5.5 in the model. Parts, but not all, of the original volume of the upper crystalline crust, are now being taken up by sediments that generate, on average, less heat, resulting in a net decrease in surface heat flow.

On the Trøndelag Platform (Fig. 5) the values of 58 mW m^{-2} from well 6610/07-02 (km 80) and the value of 68 mW m^{-2} from well 6610/07-01 are projected onto the section. The heat flow of 66 mW m^{-2} from well 6609/07-01 at the Nordland Ridge is strongly underestimated by all scenarios. The sedimentary cover is relatively thin and unlikely to contribute much heat. Only by increasing the heat generation at the top of the crystalline basement from 2.75 μW m^{-3} to 4.3 μW m^{-3} (keeping everything else unchanged) is the modelled heat flow around 66 mW m^{-2} achieved. Such a heat generation value is unusually high, however. For comparison, the Knaben Granite has a radiogenic heat generation of 3.32 μW m^{-3}, the mean for the Precambrian in southern Norway is 1.80 μW m^{-3} (Swanberg *et al.* 1974), for the Namaqua Mobile Belt 2.5 μW m^{-3} (Jones 1987) and for high-grade metamorphic rocks of the Bretagne 3.5 μW m^{-3} (Vigneresse 1988). Even if uncertainties of ±5 mW m^{-2} of the modelled heat flow and of ±4.5 mW m^{-2} of the deep-well heat flow (Table 2) are taken into account, there remains the requirement of additional heat generation around the Nordland Ridge in order to account for the observed heat flow.

The lowest heat flow encountered along the profile (Fig. 5) is from well 6607/5-1. At 43 mW m^{-2} near the Utgard High, it is largely due to a low geothermal gradient. None of the heat generation scenarios matches this heat flow either. The heat-flow uncertainty of ±2.6 mW m^{-2} (Table 2) resulting from thermal conductivity variation is relatively low since most of the sedimentary cover consists of undifferentiated Cretaceous shales. This heat-flow value is less than the one observed in the vicinity to the east, and less than expected from heat generation modelling (Fig. 5). It has already been noted, however, that this is the area where Plio/Pleistocene sediments appear to be thickest and this low heat-flow value could be explained by rapid recent sediment accumulation.

Topography and refraction. Structure, topography, and the contrast in low thermal conductivity sediments and high conductivity basement (e.g. Jaeger 1965) causes heat flow from depth to be conducted preferentially into flanking basement highs. In terms of Figure 5 this mechanism would tend to result in depressed heat-flow values associated with the central Hel Graben, Någrind Syncline, Træna and Helgeland basins, and in elevated

heat flow associated with the Vøring Marginal High, Nyk High, Utgard High and Nordland Ridge. Using a basement-to-sediment thermal conductivity contrast of two and the method of Lachenbruch (1968), Zielinski (1977) estimated up to a 30% elevation in heat flow associated with the Vøring Marginal High closest to the Vøring Escarpment.

For the three sub-basins of the Vøring Basin the ratios of the depth to basement to the half-width are about 0.2 or 0.3. Correspondingly, Von Herzen & Uyeda (1963, fig. 13) predict a 20% reduction in heat flow for the interiors of hemi-elliptical basins of this dimension and with thermal conductivity contrasts (basement: sediment) of 2. Also the Vema Dome–Rym Fault Zone–Fenris and Hel grabens system (Fig. 2a) may give rise to an increase in heat flow by refraction. Hence, this purely conductive mechanism appears capable of accounting for the increase as well as the decrease of some of the observed heat flow with respect to the heat generation models.

Hydrothermal convection. Further elevation of heat flow may result from the convective addition of heat along faults like those of the Nyk High (Fig. 5), sourced from compaction water released from the up to 5000 m thick Cretaceous shales of the Någrind Syncline and Hel Graben. The sediment cover of the eastern part of the Någrind Syncline is about 1000 m thicker than that in the western part. Particularly the thickness of Plio-/Pleistocene sediments is high in the east. This may have induced a lateral pressure gradient leading to expulsion of water towards the west if the Cretaceous shales of the Någrind Syncline are partly overpressured.

The magnitude of the heat-flow anomaly produced by water flow is strongly dependent on the flow velocity through the fault and the distribution of open fractures within the fault. The decisive parameter is evidently the degree of focusing at the fault.

In order to gain a quantitative estimate of this parameter, the simple one-dimensional model of Bredehoeft & Papadopulos (1965) is employed, which considers heat conduction with vertical fluid flow of velocity v_z to the surface $z=0$ from depth L. Zielinski & Bruchhausen (1983) showed that the resulting surface heat-flow anomaly produced by water flow is

$$\frac{HF_v}{HF_0} = \frac{\beta}{e^{\beta} - 1} \tag{9}$$

where

$$\beta = \frac{\rho_w c_w v_z L}{K} \tag{10}$$

ρ_w and c_w are the density and heat capacity of water, K is the thermal conductivity of solid, HF_0 is the original heat flow and HF_v the heat flow with convection.

If the heat flow observed, for example, over the Nyk High is 30% above average and assumed to be entirely due to vertical water flow from depth L, then $HF_v/HF_0=1.3$ and $\beta=-0.55$. If L is assumed to be 5000 m and $K=2.0$ W m^{-1}·K^{-1}, then $v_z=-5.3\times10^{-11}$ m s^{-1} (-0.17 cm a^{-1}). If $L=8000$ m and $K=1.8$ W m^{-1}·K^{-1}, then $v_z=-3.0\times10^{-11}$ m s^{-1} (-0.09 cm a^{-1}), the minus signs indicating an upward flow.

If water flow due to compaction in sedimentary basins generally has upward vertical velocities that are less than the subsidence rates (Bjørlykke 1993), then the subsidence rate v_s can be used as a base line for estimating quantitatively the minimum degree of focusing of flow required to explain the associated heat-flow anomalies. This focusing is expressed by the ratio v_z/v_s. A general subsidence rate for the Vøring Basin based on an accumulation of 8000 m of sediment in 50 Ma yields $v_s=-5.1\times10^{-12}$ m s^{-1} (-0.016 cm a^{-1}), while $v_s=-2.2\times10^{-11}$ m s^{-1} (-0.069 cm a^{-1}) is obtained for the Pleistocene maximum of about 1800 m in 2.6 Ma. For the two models, for flow velocity v_z (above), the latter results in focusing values of 2.4 and 1.3, likely to be a lower limit, while the former yields focusing values of 10 and 6, respectively. These values do not depart significantly from the proportion of basin areas to faulted basement highs exhibiting high heat flow in the Vøring Basin (Figs 2a, b, 5). However, faults in subsiding basins like the Vøring, Haltenbanken and North Sea are not likely to be open because the sediments are ductile and faults are sealing and generally less permeable than the surrounding sediments (Bjørlykke 1999; Fisher *et al.* 2003).

It has been shown earlier for the Vøring Basin that it is possible to account for a 30% increase in heat flow observed at basin-bounding basement highs by thermal refraction. Hence, apparently it is not necessary to invoke fluid flow to explain these anomalies. However, the high heat flow associated with the Nyk High (cluster 26 N, Figs 2a, b) is the result of five individual measurements, one 29 mW m^{-2} and four ranging from 86–90 mW m^{-2}. In the absence of shallow heat sources, which are unlikely in this geological setting (Vogt & Sundvor 1996), heat-flow values of these magnitudes and standard deviation become difficult, if not impossible, to explain by conductive heat transfer alone. A graphic example of this is the Brunei continental margin, of similar lithology and subsiding passively for 30 Ma (Blanche & Blanche 1997), where heat-flow values to 600 mW m^{-2} have been reported in conjunction with thermogenic hydrocarbons at the exact same site locations (Zielinski *et al.* 2003).

High heat flow and faulting is reported for much of Europe (Meier *et al.* 1979) and is attributed to fluid convection. Globally, zones of high heat flow and hydrothermal convection, such as mid-ocean ridges and geothermal areas, exhibit high variability in heat flow, decidedly skewed toward higher values (e.g. Lee & Uyeda 1965; Zielinski *et al.* 1990), not unlike the data from this study. It may be that thermal refraction of heat into the faulted basin-bounding basement highs helps create more favourable conditions for the faults to form conduits (Fisher *et al.* 2003) and to induce hydrothermal convection within them.

In summary, high heat flow and high variability (uncertainty, Table 1) of heat flow over faulted basin-bounding basement highs may be the result of hydrothermal convection and would require 5- to 10-fold focusing of vertical water flow compared with basin subsidence rates.

Magmatic processes. The effects of magmatic intrusion and crustal thinning have been modelled using a crustal stretching model. The model allows up to three crustal layers, for which conductivities, heat generation and maximum stretching factor β (McKenzie 1978) can be defined individually. The effects of underplating and sill intrusion have been modelled using a heat conduction model that allows defining the magmatic bodies at any position in the lithosphere. Values of the modelling parameters are given in Table 3.

Figure 7 shows that, irrespective of the initial conditions, heat flow returns to near-equilibrium conditions within about 50 Ma after termination of a rifting event. Naturally, equilibrium heat flow is lowest in areas of strong thinning where much of the original upper crust is compensated for by lower crust and sediments. Hence, this mechanism should have a negligible effect on the data in this study. The same applies to underplating (Fig. 8) and to sill intrusion (Fig. 9) based on their respective modelling results. It has been shown previously (Ritter *et al.* 1996) that sill intrusion leads to overmaturity of nearby source rocks but has no effect at greater distances.

Table 3. *Modelling parameters of the underplating scenarios shown in Figure 8*

Parameter	Scenario 1	2	3	4	5
Crust thickness (km)	15	15	15	15	10
Lithosphere thickness (km)	80	80	80	80	50
Depth of top intrusion (km)	15	15	15	15	10
Thickness of intrusion (km)	2.5	1	1	1	1
Temperature at base crust (°C)	650	650	650	850	850
Temperature at base lithosphere (°C)	1300	1300	1300	1300	1300
Thermal conductivity crust ($W\,m^{-1}\,K^{-1}$)	3	3	2.5	2.5	2.5
Thermal conductivity sediments ($W\,m^{-1}\,K^{-1}$)	2	2	1.2	1.2	1.2
Thermal conductivity mantle ($W\,m^{-1}\,K^{-1}$)	6	6	6	6	6
Beta factor whole lithosphere	2	2	2	2	2

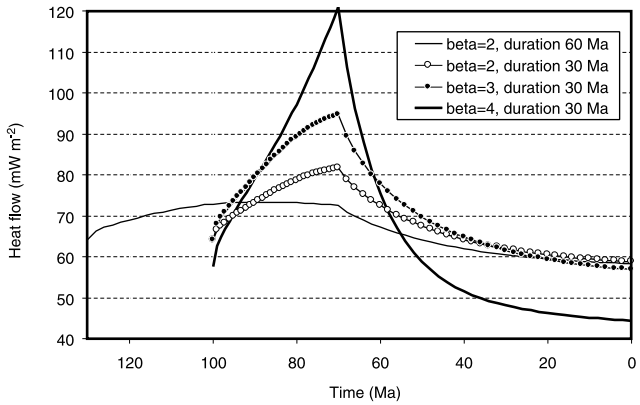

Fig. 7. Heat-flow histories derived from different β factors. Pre-rifting crustal conditions calibrated against Trøndelag Platform. One-dimensional finite element model. Initial lithospheric thickness 100 km, initial crustal thickness 30 km, duration of rifting 30 (60) Ma. Temperature at base lithosphere 1300°C.

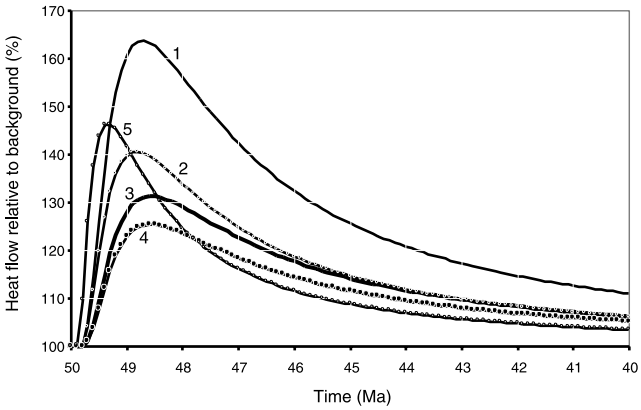

Fig. 8. Surface heat flow generated by accumulation of 1 km and 2.5 km thick magmatic bodies at the base of the crust (underplating), modelled for different scenarios. Posted numbers refer to scenario ID (see Table 3 for modelling conditions). Instantaneous intrusion.

CONCLUSIONS

This paper presents a new dataset of heat flow for the Mid-Norwegian Shelf and discusses it in terms of processes that may influence the observed variability. This is relevant to petroleum exploration since temperature is the prime parameter that influences source-rock maturation. In addition, zones of high heat flow may identify possible surface expressions of conduits for active fluid migration. Such conduits have been shown to be pathways along which hydrocarbons tend to

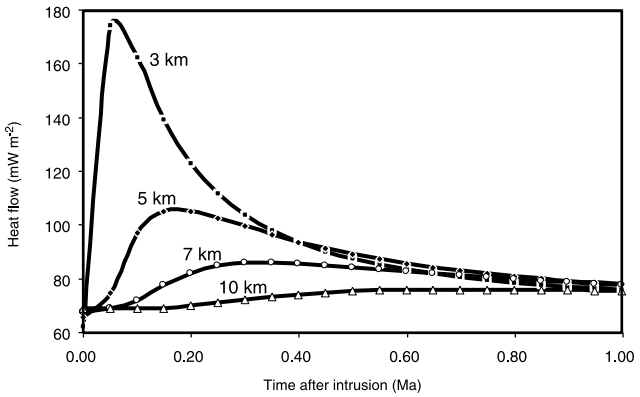

Fig. 9. Surface heat flow generated by a 100 m thick sill intruded at various depth levels and average thermal background conditions. Background heat flow prior to rifting 60 $mW\,m^{-2}$, temperature of intrusion 1200 °C. Remaining parameters as in Table 3, scenario 1.

accumulate (Zielinski & Bruchhausen 1983; Zielinski *et al.* 1985, 1990) and/or leak to the surface (Zielinski *et al.* 2003).

Relatively isolated high heat flow observed at shallow water depths may be an artefact of bottom water disturbances. However, such anomalies are also observed at greater depths where this mechanism is unlikely, and those anomalies have been attributed there to vertical fluid migration (Sundvor *et al.* 1989, 2000; Vogt & Sundvor 1996). Short wavelength heat-flow variations appear to be controlled structurally and can be explained by sedimentation and thermal refraction effects. Refraction of heat into fault zones may contribute to the observed high heat flow, provide more favourable conditions for the faults to become conduits (Fisher *et al.* 2003) and induce hydrothermal convection within the faults. Marine heat-flow measurements may provide valuable evidence for the role of faults in fluid and heat transfer in sedimentary basins, traditionally investigated via alternate approaches (Bjørlykke 1999; Fisher *et al.* 2003).

Submarine avalanches seem not to be important in this survey area, but may have affected parts of the data of Sundvor *et al.* (1989) collected further south. Neither crustal thinning, underplating, nor sill intrusion would have a measurable effect on present-day heat flow, if it occurred more than 50 Ma ago. The net effect of crustal thinning may be a reduction of the crustal heat generation potential, since the accumulating sediments cannot compensate fully for the lost heat generation from a crystalline basement.

In consequence, high heat flow of the Vøring Marginal High may be a combined effect of thermal refraction into high-conductivity volcanics and water flow along faults of the

Vøring Escarpment. The extreme variability of Hel Graben and Nyk High heat flow may be caused by thermal refraction away from that basin and pore-water drainage along the numerous faults of the area. The unusually low heat flow of the Någrind Syncline area may be caused by reduced crustal heat generation and some thermal refraction into the Utgard High. The heat flow of the Trøndelag Platform can be explained by crustal heat generation and some minor convection along relatively shallow faults.

The results and conclusions presented in this paper are mainly from two projects, 'Heat Flow Measurements Vøring Basin 1994' and 'Vøring Basin Analysis Program, Phase 1'. These projects were funded by Mobil Exploration Norway Inc., Saga Petroleum a.s., Statoil, Conoco Norway Inc., Phillips Petroleum Company Norway and IKU (now SINTEF) Petroleum Research. Oceanographic data were provided by Svein Østerhus, Department of Physical Oceanography, University of Bergen. The transient effects of water temperature variations on geothermal gradients were calculated by Geir Owren, SINTEF Refrigeration Engineering. The field operation was carried out using the Norwegian research vessel *M/S Geo Boy*. The marine heat-flow measurements were performed by Omegalink International Ltd. The authors thank K. Bjørlykke and E. Sundvor for their reviews, which led to improvements in the original manuscript.

REFERENCES

Bjørlykke, K. 1993. Fluid flow in sedimentary basins. *Sedimentary Geology,* **86**, 137–158.

Bjørlykke, K. 1999. Principal aspects of compaction and fluid flow in mudstones. *In:* Halpin, A.C., Fleet, A.J. & Macquaker, J.H.S. (eds) *Muds and mudstones: physical and fluid flow properties.* Geological Society, London, Special Publications, **158**, 73–78.

Blanche, J.B. & Blanche, J.D. 1997. An overview of the hydrocarbon potential of the Spratly Islands archipelago and its implications for regional development. *In:* Fraser, A.J., Matthews, S.J. & Murphy, R.W. (eds) *Petroleum geology of southeast Asia.* Geological Society, London, Special Publications, **126**, 293–310.

Blystad, P., Brekke, T., Færseth, R.B., Larsen, B.T., Skogseid, J. & Tørudbakken, B. 1995. Structural Elements of the Norwegian Continental shelf, Part 2, the Norwegian Sea. *NPD Bulletin,* **8**.

Bredehoeft, J.D. & Papadopulos, I.S. 1965. Rates of vertical groundwater movement estimated from the earth's thermal profile. *Water Resources Research,* **1**, 325–328.

Brekke, H., Dahlgren, S., Nyland, B. & Magnus, C. 1999. The prospectivity of the Vøring and Møre basins on the Norwegian Sea continental margin. *In:* Fleet, A.J. & Boldy, S.A.R. (eds) *Petroleum Geology of Northwest Europe, Proceedings of the 5th Conference.* Geological Society, London, 261–274.

Bugge, T. 1983. *Submarine slides on the Norwegian continental margin, with special emphasis on the Storegga area.* IKU Publication, **110**.

Bugge, T., Befring, St & Belderson, R.H. 1987. *et al.* A giant three-stage submarine slide off Norway. *Geo-Marine Letters,* **7**, 191–198.

Buntebarth, G. 1980. *Geothermie. Eine Einführung in die allgemeine und angewandte Wärmelehre des Erdkörpers.* Springer-Verlag, Berlin.

Cermak, V., Bodri, L., Rybach, L. & Buntebarth, G. 1990. Relationship between seismic velocity and heat production: comparison of two sets of data and test of validity. *Earth and Planetary Science Letters,* **99**, 48–57.

Eldholm, O., Thiede, J. & Taylor, E. 1987. *et al. Proceedings of the Ocean Drilling Program, Initial Report,* **104, Pt. A**.

Eldholm, O., Thiede, J. & Taylor, E. 1989. Evolution of the Vøring volcanic margin. *In:* Eldholm, O., Thiede, J. & Taylor, E. (eds) *Proceedings of the Ocean Drilling program, Scientific Results,* **104**, 1033–1065.

Fisher, Q.J., Casey, M., Harris, S.D. & Knipe, R.J. 2003. Fluid-flow properties of faults in sandstone: the importance of temperature history. *Geology,* **31**, 965–968.

Gammelsrød, T. & Holm, A. 1984. Variations of temperature and salinity at Station M (66°N 02°E) since 1948. *Rapports et Procès-verbaux Des Réunions. Conseil International Pour L'exploration De La Mer [International Council for the Exploration of the Sea],* **185**, 188–200.

Gammelsrød, T., Østerhus, S. & Godøy, Ø. 1992. Decadal variations of ocean climate in the Norwegian Sea observed at Ocean Station 'Mike' (66°N 2°E). *ICES Marine Science Symposium,* **195**, 68–75.

Haenel, R. 1974. Heat flow measurements in the Norwegian Sea, 1974. *Meteor Forschungsergebnisse Reihe C,* **17**, 74–78.

Heier, K.S. & Grønlie, G. 1977. Heat flow-heat generation studies in Norway. *In:* Saxena, S.K. & Bhattacharji, S. (eds) *Energetics of geological processes.* Springer-Verlag, New York, 217–235.

Hurtig, E., Cermak, V., Haenel, R. & Zui, V. 1992. *Geothermal Atlas of Europe.* GeoForschungszentrum Potsdam, Publication No, **1**.

Jaeger, J.C. 1965. Application of the theory of heat conduction to geothermal measurements. *In:* Lee, W.H.K. (ed.) *Terrestrial heat flow.* American Geophysical Union, Geophysical Monograph Series, **8**, 7–23.

Jones, M.Q. 1987. Heat flow and heat production in the Namaqua Mobile Belt, South Africa. *Journal of Geophysical Research,* **92** (B7), 6273–6289.

Lachenbruch, A.H. 1968. Rapid estimation of the topographic disturbance to superficial thermal gradients. *Reviews of Geophysics,* **6**, 365–400.

Lachenbruch, A.H. & Sass, J.H. 1977. Heat flow in the United States and the thermal regime of the crust. *In:* Heacock, J.G. (ed.) *The earth's Crust: its nature and physical properties.* American Geophysical Union Geophysical Monograph Series, **20**, 626–675.

Langseth, M.G. & Zielinski, G.W. 1974. Marine heat flow measurements in the Norwegian–Greenland Sea and in the vicinity of Iceland. *In:* Kristjansson, L. (ed.) *Geodynamics of Iceland and the North Atlantic area.* NATO Advanced Study Institute Series C, **11**. D. Reidel, Dordrecht, Boston, 277–295.

Lee, W.H.K. & Uyeda, S. 1965. Review of heat flow data. *In:* Lee, W.H.K. (ed.) *Terrestrial heat flow.* American Geophysical Union Geophysical Monograph Series, **8**, 87–190.

McKenzie, D. 1978. Some remarks on the development of sedimentary basins. *Earth and Planetary Science Letters,* **40**, 25–32.

Meier, R., Hurtig, E. & Ludwig, A. 1979. Fault tectonics and heat flow in Europe. *In:* Cermak, V. & Rybach, L. (eds) *Terrestrial heat flow in Europe.* Springer-Verlag, Berlin, 112–118.

Pedersen, T. & Skogseid, J. 1989. Vøring Plateau Volcanic Margin: Extension, Melting and Uplift. *In:* Eldholm, O., Thiede, J. & Taylor, E. (eds) *Proceedings of the Ocean Drilling Program, Scientific Results,* **104**.

Ratcliffe, A.E. 1960. The thermal conductivities of ocean sediments. *Journal of Geophysical Research,* **65**, 1535–1541.

Ritter, U., Myhr, M. B. & Mukhopadhyay, M. 1996. Thermal history and hydrocarbon generation modelling in parts of the Vøring Basin, Norwegian Sea. Paper L012, presented at the EAGE 58th Annual Technical Conference, 3–7 June, Extended Abstracts, 2.

Schenk, H.J., Horsfield, B., Krooss, B. & Schaefer, R.G. 1997. Kinetics of Petroleum Formation and Cracking. *In:* Welte, D.H., Horsfield, B. & Baker, D.R. (eds) *Petroleum and Basin Evolution*, 231–269.

Skogseid, J., Pedersen, T. & Larsen, V. 1992. Vøring Basin: subsidence and tectonic evolution. *In:* Larsen, R.M., Brekke, H., Larsen, B.T. & Talleraas, R. (eds) *Structural and Tectonic Modelling and its Application to Petroleum Geology.* NPF Special Publication. Elsevier, Amsterdam, 55–82.

Stuevold, L.M., Skogseid, J. & Eldholm, O. 1992. Post Cretaceous uplift events of the Vøring continental margin. *Geology,* **20**, 919–922.

Sundvor, E., Myhre, A.M. & Eldholm, O. 1989. Heat flow measurements on the Norwegian continental margin during the FLUNORGE project. *University of Bergen Seismo-Series,* **27**.

Sundvor, E., Eldholm, O., Gladczenko, T.P. & Planke, S. 2000. Norwegian–Greenland Sea thermal field. *In:* Nøttvedt, A., Larsen, B.T., Gabrielsen, R.H., Olaussen, S., Brekke, H. & Tørudbakken, B. (eds) *Dynamics of the Norwegian Margin.* Geological Society, London, Special Publications, **167**, 397–410.

Swanberg, C.A., Chessman, M.D., Simmons, G., Smithson, S.B., Grønlie, G. & Heier, K.S. 1974. Heat flow – heat generation studies in Norway. *Tectonophysics,* **23**, 31–48.

Tissot, B. & Espitalié, J. 1975. L'evolution thermique de la matière organique des sediments: applications d'une simulation mathematique. *Revue de l'Institut Français du Pétrole,* **30**, 743–777.

Van Schaack, M., Wheeler, W., Gabrielsen, R., Karpuz, R., Mjelde, R. & Reemst, P. 1998. Geometries of crustal underplating along the Vøring Margin – Significance for basin evolution models. Paper 3-03, presented at the 60th EAGE Annual Conference and Technical Exhibition, Leipzig, June, Extended Abstracts.

Vigneresse, J.L. 1988. Heat flow, heat production and crustal structure in the peri-Atlantic regions. *Earth and Planetary Science Letters,* **87**, 303–312.

Vogt, P.R. & Sundvor, E. 1996. Heat flow highs on the Norwegian–Barents–Svalbard continental slope: deep crustal fractures, dewatering, or 'memory in the mud'? *Geophysical Research Letters,* **23**, 3571–3574.

Von Herzen, R.P. & Maxwell, A.E. 1959. The measurement of thermal conductivity of deep-sea sediments by a needle probe method. *Journal of Geophysical Research,* **64**, 1557–1563.

Von Herzen, R.P. & Uyeda, S. 1963. Heat flow through the Eastern Pacific ocean floor. *Journal of Geophysical Research,* **68**, 4219–4250.

Zielinski, G.W. 1977. *Thermal evolution of the Norwegian–Greenland Sea and its rifted continental margin.* PhD thesis. Columbia University.

Zielinski, G.W. 1979. On the thermal evolution of passive continental margins, thermal depth anomalies, and the Norwegian–Greenland Sea. *Journal of Geophysical Research,* **84**, 7577–7588.

Zielinski, G.W. & Bruchhausen, P.M. 1983. Shallow temperatures and thermal regime in the hydrocarbon province of Tierra del Fuego. *American Association of Petroleum Geologists Bulletin,* **67**, 166–177.

Zielinski, G.W., Drahovzal, J.A., DeCoursey, G.M. & Ruperto, J.M. 1985. Hydrothermics in the Wyoming overthrust belt. *American Association of Petroleum Geologists Bulletin,* **69**, 699–709.

Zielinski, G.W., Nassaur, F.J., Zielinski, R.L.B., Lindgren, M.G. & Raetz, U.S. 1990. Heat flow measurements in early exploration strategy. *Geological Journal, Ukrainian Academy of Sciences,* **1**, 33–39.

Zielinski, G. W., Bjorøy, M. & Zielinski, R. L. B. 2003. Heat flow and surface geochemistry in the Brunei continental margin. Abstract presented at the American Association of Petroleum Geologists Annual Convention, 11–14 May.

Received 26 November 2003; revised typescript accepted 6 August 2004.